Synthesis, Structure and Thermal Properties of Volatile Group 11 Triazenides as Potential Precursors for Vapor Deposition

Rouzbeh Samii,[1] Anton Fransson,[1] David Zanders,[2,3] Atilla Varga,[2] Seán T. Barry,[2] Lars Ojamäe,[1] Vadim Kessler,[4] and Nathan J. O'Brien[1,*]

[1]Department of Physics, Chemistry and Biology, Linköping University, Linköping SE-58183, Sweden

[2]Department of Chemistry, Carleton University, 1125 Colonel By Drive, Ottawa, Ontario, K1S 5B6, Canada

[3]Faculty of Chemistry and Biochemistry, Ruhr University Bochum, Bochum, 44801, Germany

[4]Department of Molecular Sciences, Swedish University of Agricultural Sciences, P.O. Box 7015, 75007 Uppsala, Sweden

*E-mail: nathan.o.brien@liu.se

Abstract

Group 11 thin films are desirable as interconnects in microelectronics. Although many M–N bonded Cu precursors have been explored for vapor deposition, there is currently a lack of suitable Ag and Au derivatives. Herein, we present monovalent Cu, Ag and Au 1,3-di-*tert*-butyltriazenides that have potential for use in vapor deposition. These compounds possess thermal stability and volatility that rival that of current state-of-the-art group 11 precursors with bidentate M–N bonded ligands. All compound sublime quantitatively between 120 and 130 °C at 0.5 mbar. Thermogravimetric analysis showed the Cu and Ag compounds both volatilized at ~200 °C with 0 and 2% residual mass, respectively. The Au triazenide showed two separated mass loss events at ~175 and 240 °C, and 35% residual mass. The crystal structure of the Cu compound showed a dimer, whilst the Ag and Au derivatives were tetrameric. Nuclear magnetic resonance spectroscopy showed dimers for the Cu and Au compounds and a dimer/tetramer equilibrium for the Ag compound. Electronic energies from density functional theory calculations confirmed dimeric preference for the Cu triazenide while Ag and Au preferred the tetrameric. However, all three compounds showed dimeric preference when accounting for entropy. Dimers are, therefore, expected to dominate in the gas phase for all three compounds during sublimation. Natural bond orbital analysis was used to identify orbital interactions important for the dimer/tetramer preference. Three factors were identified, in conjunction with strong metal-metal interactions, to increase the preference for rhombic tetramers.

Introduction

Thin films of group 11 metals are highly desirable as interconnects in integrated circuits due to their excellent electrical and thermal conductivity, and resistance to electron migration.[1] Furthermore, transparent Ag thin film electrodes have potential for solar cell applications,[2] whilst Au is advantageous for chemical and biological sensors.[3] Today, Cu, Ag and Au films are commonly deposited by vapor deposition techniques.[4,5] Chemical vapor deposition (CVD) and atomic layer deposition (ALD) are two methods currently used to deposit high quality thin films of group 11 metals. To be successful, both methods require precursors that are sufficiently volatile and thermally stable for transport from the source to the reaction chamber without decomposing. In CVD, the precursors are mixed in the reaction chamber and react in the gas phase to deposit the target material. In ALD, the precursors are added to the system sequentially to allow the process to be governed by self-limiting surface reactions. To date, there are more precursors known for Cu in comparison to Ag and Au, and thus less deposition processes are reported for the latter metals.

The amidinate ligand system has been used to produce volatile and thermally stable transition metal precursors for vapor deposition (Figure 1a).[6–8] A drawback of amidinate precursors is their tendency to decompose *via* two pathways: β-hydride elimination and carbodiimide (CDI) de-insertion.[9,10] While β-hydride elimination is easily blocked by having exocyclic *N*-substituents free from β-hydrogens, suppressing CDI de-insertion is more difficult as it involves the substituent on the endocyclic carbon. Metallic Cu films have been deposited by ALD using Cu(I) amidinates.[6,11–18] However, the Ag(I) and Au(I) amidinates are thermally unstable with respect to CDI de-insertion and therefore have not been successfully used for vapor deposition.[10,19] The iminopyrrolidinates are mono-cyclic amidinates, where the ligand backbone and carbon substituent form a pyrrolidine ring (Figure 1b).[9] Tethered to a nitrogen in the ligand backbone, the substituent on the endocyclic carbon is difficult to access for CDI de-insertion, making the iminopyrrolidinates more thermally stable than the acyclic amidinates.[10] Thus, not only have the monovalent group 11 iminopyrrolidinates afforded Cu films by ALD,[20] but also Ag and Au films, with ~3 at. % carbon, by low-temperature CVD.[5] Further constrained, bicyclic amidinates have been used to yield monovalent group 11 compounds with improved thermal stability over the iminopyrrolidinates (Figure 1c).[21,22] Using these compounds with H_2 afforded Ag and Au films with ~6–7 at. % carbon by low-temperature CVD.[22]

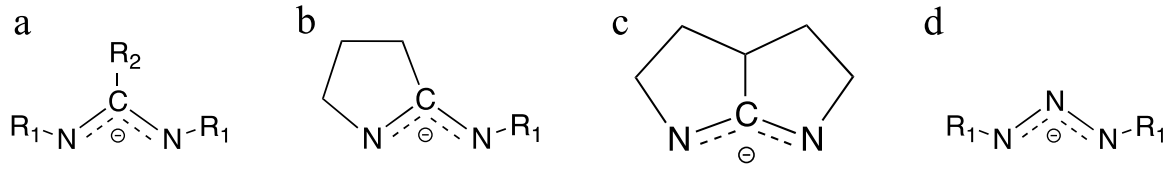

Figure 1: General structure of the bidentate N–M bonded a) acyclic amidinates, b) mono-cyclic iminopyrrolidinates, and c) bicyclic amidinate ligands, and triazenide ligand. R_1 = alkyl, R_2 = H or Me.

An alternative approach to develop new M–N bonded precursors is to alter the N–C–N ligand backbone. The triazenides differ from the amidinates by replacing the substituent on the endocyclic carbon with a nitrogen atom (Figure 1d). This change in the ligand backbone replaces substituted carbon with a lone pair and blocks decomposition *via* mechanisms resembling the CDI de-insertion. Monovalent group 11 triazenides exist in the literature.[23–28] All except one of these known triazenides have 1,3-diaryltriazenide ligands and are therefore not suitable for vapor deposition. The exception is a tetrameric Cu(I) compound with 1,3-dimethyltriazenide ligands, where only melting point (185–186 °C) and structural data has been discussed.[29,30]

Recently, we reported the first examples of volatile group 13 and 14 dialkyltriazenides.[31–34] The Ga and In triazenides have been used as ALD precursors to afford excellent quality GaN, InN, InGaN and In_2O_3.[31,32,35,36] With the success of the triazenide ligand to produce volatile and thermally stable group 13 and 14 compounds, we decided to investigate its reactivity with monovalent coinage metals. Herein, we report the synthesis, structure, and thermal properties of monovalent group 11 triazenides. Their ease to produce, high volatility and thermal stability makes these new precursors highly interesting for use in vapor deposition.

Results and Discussion

Compounds **1**–**3** were obtained in good yields by reacting MCl (M = Cu, Au, Ag) with lithium 1,3-di-*tert*-butyltriazenide[34] in THF followed by recrystallization (Scheme 1). The compounds were fully characterized by nuclear magnetic resonance (NMR), elemental analysis, decomposition points, and X-ray crystallography. Crystals of **1**–**3** did not degrade when stored for weeks under ambient conditions. When immersed in water for two weeks, **1** showed slight green discoloration whilst **2** and **3** remained unchanged.

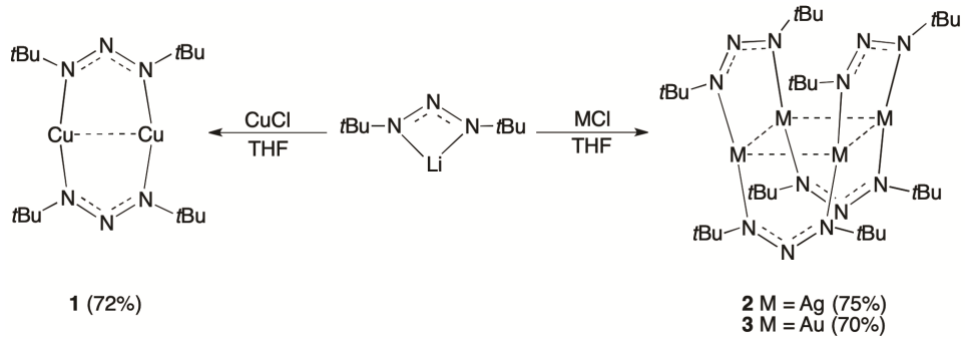

Scheme 1: Synthesis of Cu, Ag and Au triazenides **1**–**3**.

The ^{1}H NMR spectra of **1**–**3** in C_6D_6 all showed a singlet at 1.27 ppm, which is consistent with the dimer structure. Compound **2** also gave an additional singlet for the tetrameric structure at 1.43 ppm. The dimer/tetramer ratio of **2** changed when varying the concentration of the NMR sample (Figure 2a). As the total concentration of **2** is increased, the relative concentration of tetramer increases as expected. Analysis of **2** (13.3 mM) in a coordinating solvent (THF-d_8) did not change the dimer/tetramer equilibrium (see supporting information). Using the data, the ambient temperature dissociation constant of **2**, K_{diss}, was estimated to be 28.7±0.4 mM. Variable temperature NMR analysis on a 3.8 mM sample of **2** showed the equilibrium slowly shift to the dimer for spectra acquired between 30 and 60 °C (Figure 2b). A van't Hoff plot of $\ln[K_{diss}(T)]$ vs. T^{-1} gave ΔH and ΔS of dissociation of –38.6 kJ mol^{-1} and 98.9 J K^{-1} mol^{-1}, respectively (see supporting information). The NMR data indicates that **1** and **3** are predominantly dimeric in solution whilst **2** exists in a dimer/tetramer equilibrium. Similar dimer/tetramer and dimer/trimer equilibria were found for known Ag formamidinate[37] and Ag acetamidinate[7] compounds, respectively.

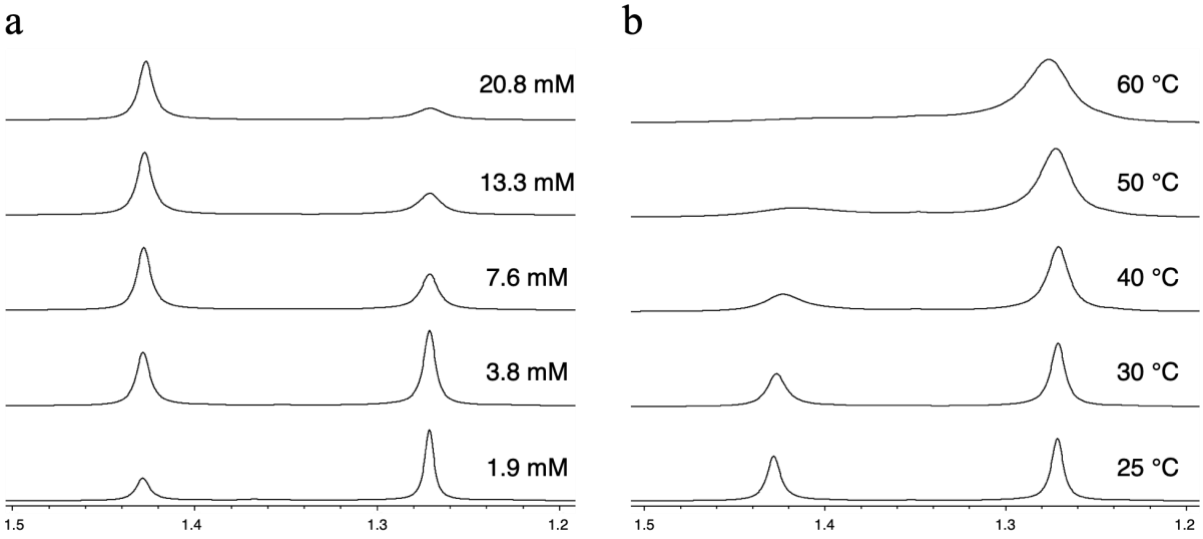

Figure 2. The effect of a) concentration and b) temperature (3.8 mM sample) on the dimer/tetramer ratio of **2**.

The crystal structure of **1** showed a dimer with two bridging 1,3-di-*tert*-butyltriazenide ligands on opposite sides of the metal centers forming a planar metallacycle (Figure 3). All Cu–N and N–N bond lengths are equivalent, indicating the electrons are delocalized over the Cu and N centers. This structure is consistent with the 1,3-bis(2,6-diisopropylphenyltriazenide) ($dipp_2N_3$) analog, which has the aromatic rings non-coplanar to the metallacycle. Interestingly, the 1,3-diphenyltriazenide (dpt) analog showed two sets of Cu–N and N–N bond lengths and the aromatic rings were in-plane with the metallacycle.[23,27]

Table 1: Bond parameters for **1** and its diphenyl and di(2,6-diisopropylphenyl) triazenide analogs.

	1	dpt Cu	$Dipp_2N_3$ Cu
Cu···Cu	2.443	2.45	2.446
Cu–N	1.883	1.899, 1.939	1.882
N–N	1.292	1.274, 1.316	1.303
N–Cu–N	172.96	171.8	172.63
N–N–N	117.73	115.8	115.53

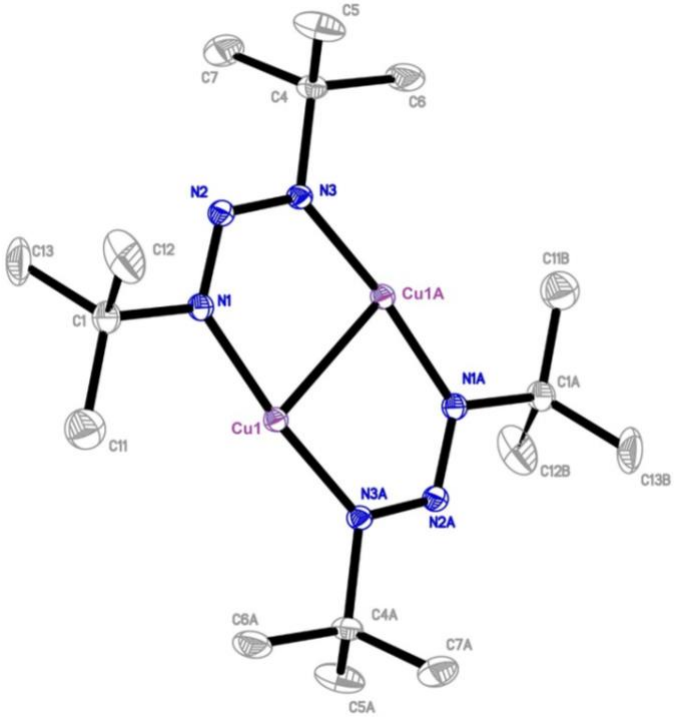

Figure 3: ORTEP drawing of **1**. Thermal ellipsoids at the 50% probability level. All hydrogen atoms were omitted for clarity.

The crystal structures of **2** and **3** showed tetramers with the four metal centers in a rhombus- and buckled square conformation, respectively (Figure 4). Four 1,3-di-*tert*-butyltriazenide ligands bridge the metal centers along the perimeter, alternating above and below the plane. In the structure of **3**, the ligands are twisted relative to the metal centers they bridge, while **2** showed only minor twisting (N–M···M–N: 18.0 and 2.57°, respectively). The bond parameters for **2** and **3** are given in Table 2. The Ag 4-fluorophenyltriazenide (4F-dpt) analog is the only other known tetrameric Ag triazenide and also adopts the rhombus conformation.[28] Compared to the 4F-dpt analog, **2** has slightly longer M···M edge distances. However, **2** has smaller acute M···M···M angles and therefore a significantly shorter M···M. The M···M diagonal in **2** is only 0.1 Å longer than the average M···M edge distance.

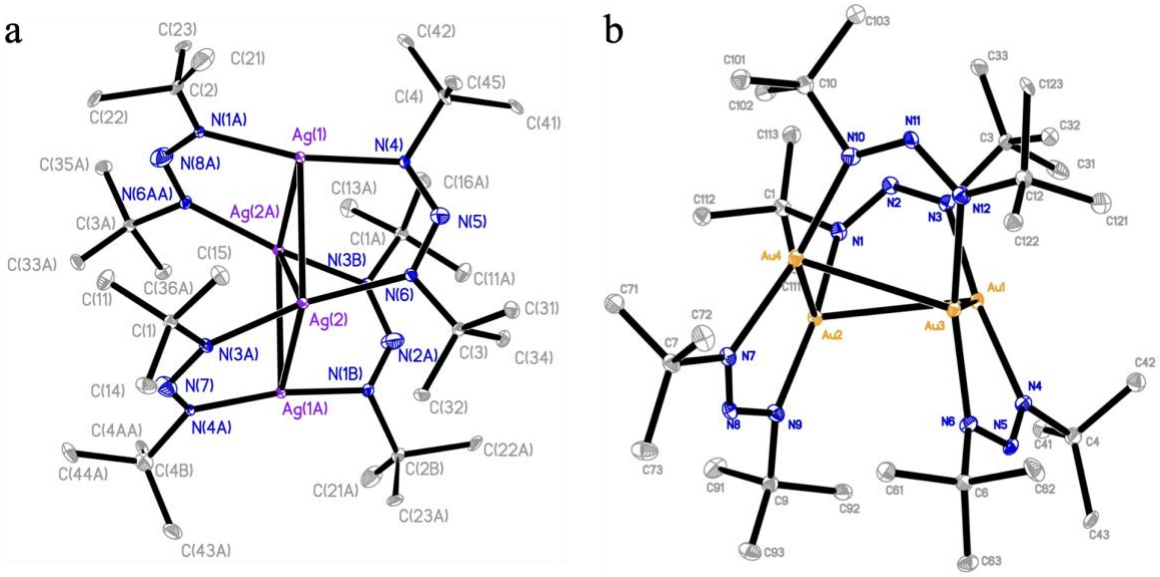

Figure 4: ORTEP drawings of the crystal structures for a) **2** and b) **3** with thermal ellipsoids at the 30% probability level. All hydrogen atoms were omitted for clarity.

Compound **3** showed a significant difference in N–N lengths for two of the ligands on the opposite edge of the buckled square (0.108 and 0.066 Å). A similar, albeit smaller, difference was found in the Au diphenylacetamidinate, which also adopted the buckled square conformation.[38] In contrast to **3**, the dpt Au analog adopts a rhombus conformation and has shorter M···M edge.[24] Compound **3** may adopt the buckled square conformation over the rhombic due to steric effects caused by the bulky *tert*-butyl groups. Similar buckled square conformation is found in tetrameric Cu and Ag compounds employing triazenide and bicyclic guanidinate-like ligands, respectively, and are attributed to steric effects.[26,39] However, **2** and **3** have comparable M–N and M···M lengths, and are therefore expected to adopt the same conformation by steric arguments alone. Thus, electronics are also likely to influence the

dimer/tetramer preference of **1-3** and other similar compounds. For example, the crystal structures of Ag dpt and 4F-dpt analogs show dimers and tetramers, respectively, despite having ligands of similar size.[26,28]

Table 2: Average bond lengths (Å) and angles (°) from crystal structures of **2** and its di(4-fluorophenyl) analog, and **3** and its diphenyl analog.

	2	4F-dpt Ag	**3**	dpt Au
(edge) M···M	2.910	2.821	2.921	2.850
(diag.) M···M	3.016	3.288	4.043	3.320
M–N	2.116	2.128	2.046	2.041
N–N	1.297	1.293	1.285[1]	1.285
M···M···M[2]	62.43, 117.57	71.30, 108.70	87.59	71.23, 108.62
M–N–M	162.62	177.7	168.52	176.63
N–N–N	118.51	118.0	119.16	118.67
N–M···M–N	2.57	0.43	18.0	3.87[3]

[1] One bond length is significantly shorter than the other (1.203 Å). Omitting the shorter bond gives an average d = 1.297 Å.

[2]The rhombic structures have two distinct angles.

[3] Two of the ligands are significantly more tilted than the other two (0.74 and 0.34, and 6.26 and 8.14).

DFT and NBO calculations

The DFT geometries of **1**–**3** are in good agreement with their respective crystal structures (see supporting information). Compound **2** showed the largest deviation, where the optimized geometry gave Ag···Ag···Ag angles closer to 90° and, consequently, a longer diagonal Ag···Ag distance compared to the crystal structure (see supporting information). Structures were also optimized for dimeric **2** and **3**, and rhombic **1** and **3**. The electronic energy difference ΔE_0 between the dimeric and tetrameric structures are estimated as

$$\Delta E_0 = E_0(\text{tetramer}) - 2E_0(\text{dimer})$$

where E_0 is the electronic energies of the optimized structures. The ΔE_0 increased in the order **1** < **2** < **3**. Dimeric **1** was slightly favored over rhombic **1**, while **2** and **3** favored the rhombic structures. The ΔE_0 difference was negligible between rhombic and buckled square **3**.

Due to the decrease in entropy upon combining two dimers into a tetramer, the difference in Gibbs free energy (ΔG) for **1**–**3** (calculated analogously to ΔE_0) favors the dimeric structures in the gas phase and increased in the same order as ΔE_0.

Table 3: ΔE_0 and ΔG (kcal mol^{-1}) between the tetrameric and two dimeric structures for **1**–**3**.

	1	**2**	**3**
ΔE_0	-1.05	-6.51	-15.5
ΔG	17.2	14.5	7.94

Dimers are therefore expected to dominate in the gas-phase, and if present, the concentration of tetrameric species would increase in the order **1** < **2** < **3**. However, in a solution of benzene, NMR experiments showed a significant presence of tetrameric **2** and none for **1** and **3**. The inconsistency between DFT and observations from NMR may arise from solvation. Still, the inconsistency remained after accounting for solvation in benzene using a polarizable continuum model.

The optimized structures of **1**–**3** were investigated by natural bond orbital (NBO) analysis. Natural bond orders for dimeric **1**–**3** from natural resonance theory calculations agree with the expected formal bond orders. The M–N bonds showed high ionic character, ~100, 84, and 74% for dimeric **1**, **2**, and **3**, respectively. Wiberg bond indices for the structures of **1**–**3** ranged between 0.05 to 0.1 (see supporting information). The metal center natural charges for **1**–**3** decreased in the order **1** > **2** >> **3** (Table 4), as expected based on electron affinities for Cu–Au. Rhombic **1** gave ~0.02 greater charge than the dimeric structure. The opposite was found for **2** and **3**, but with smaller differences compared to **1** (<0.01).

Table 4: Average natural charges for the metal center (M), triazenide backbone (N_3), and ligands (R-group) for dimeric and tetrameric **1**–**3**.

	Dimeric			Rhombic			Square
	1	**2**	**3**	**1**	**2**	**3**	**3**
M	0.655	0.635	0.491	0.678	0.627	0.489	0.487
N_3	-0.961	-0.931	-0.831	-0.993	-0.937	-0.834	-0.830
R-group	0.153	0.148	0.170	0.158	0.155	0.172	0.172

Second order perturbation theory analysis (donor-acceptor interactions) from the NBO calculations were used to compare stabilization energies ($E^{(2)}$) for donor-acceptor interactions for rhombic **1**–**3** with two of their respective dimers. The $\Delta E^{(2)}$ was estimated as

$$\Delta E^{(2)} = E^{(2)}(Rhombic) - 2E^{(2)}(Dimeric)$$

and was used to compare interactions in dimers with their equivalent tetrameric. Interactions involving valence acceptor orbitals stabilized dimers more than tetramers ($\Delta E^{(2)} < 0$ kcal mol^{-1}) due to more favorable orbital overlap. For example, geminal $n1_N \rightarrow n^*_M$ (which is essentially σ_{MN}) greatly favored dimeric **1**–**3** over rhombic, and $\Delta E^{(2)}$ decreased in the order **3** < **2** < **1** (Table 5). Dimers were favored for interactions involving valence acceptors where the number of interactions remained unchanged between two dimeric- and a rhombic structure (e.g. geminal M–L). The geminal M–M interactions, however, favored the rhombic structures as they compensated for their lower $E^{(2)}$ by having a larger number of interactions.

Interactions involving Rydberg acceptor orbitals often favored the rhombic over dimeric ($\Delta E^{(2)} < 0$ kcal mol^{-1}), as the orbital overlap was similar, or sometimes even larger for the rhombic structures. Vicinal and remote interactions benefited the rhombic structures due to their larger number of interactions over dimers. In contrast to **2** and **3**, structures of **1** interacted poorly with Rydberg acceptors and gave modest $\Delta E^{(2)}$. Therefore, rhombic **1** was not stabilized sufficiently to compensate for the destabilization relative to dimeric 1 (e.g. $n1_N \rightarrow n^*_M$) while Rydberg acceptors had larger impact on rhombic **2** and **3**. This may explain why the crystal structure of **1** showed dimers while **2** and **3** were tetrameric. See the supporting information for more details on the NBO analysis.

Table 5: $\Delta E^{(2)}$ (kcal mol^{-1}) for two interactions involving valence acceptor orbitals and two involving Rydberg acceptor orbitals **1**–**3**.

	$n1_N \rightarrow n^*_M$	$n^{sd}_M \rightarrow n^*_M$	$n^{sd}_M \rightarrow RY1_N$	$n^{sd}_M \rightarrow RY3_N$
1	-146	3.81	-2.87	3.43
2	-98.9	34.8	38.9	48.8
3	-55.5	3.35	7.15	39.9

To summarize, the rhombic structures must adapt and retain orbital overlap from the dimeric structure, particularly for the geminal M–N. Strong M–M interactions favors the rhombic structures as the they have more of these interactions compared to two dimers. For the same reason, strong vicinal and remote interactions favor the rhombic structures. Lastly, if accessible, Rydberg acceptor levels are highly impactful, favoring the rhombic structures by having comparable orbital overlap between the dimeric and rhombic structure.

Thermal analysis

Compound **1**–**3** sublimed quantitatively between 120 and 130 °C at 0.5 mbar. The TGA ramp experiments of **1** and **2** (with 10 mg samples) showed one-step volatilizations at ~200 °C with 0 and 2% residual mass, respectively. The derivative curve of **1** showed ideal volatilization kinetics. Meanwhile, **2** volatilized in a non-ideal manner, which may be caused by a two-step mechanism where tetramers first form dimers which then volatilize. A similar two-step process was postulated for the bicyclic Ag amidinate to explain why the volatilization kinetics resembled that of the dimeric bicyclic Cu amidinate.[22] Compound **3** showed two well defined mass loss events with onsets at ~175 °C and ~240 °C and a residual mass of 35%.

Compounds **1** and **2** were stress tested by performing TGA ramp experiments with 20 and 40 mg samples. Larger samples normally take longer to completely volatilize and are therefore exposed to higher temperatures, which is observed as a shift in the mass loss curve towards higher temperatures. If the compound is thermally unstable at the elevated temperature, the mass loss rate will show irregularities and the residual mass will increase for larger samples.

Compound **1** showed irregularities in the derivative curve at ~230 °C for 20 and 40 mg samples, coinciding with the melting point (229–230 °C). The irregularities may be explained by melting of the sample, considering the residual mass remained low (<0.5%). Also, larger samples of **1** gave the typically observed shift in the mass loss curve to higher temperature. In contrast, the mass loss curve of **2** did not shift to higher temperature for larger samples. Initially, the curves are displaced for larger samples, however, above ~210 °C, the mass loss rate increases faster for the larger samples, resulting in all ramp experiments plateauing at similar temperatures (See supporting information). The absence of shift may be explained by the tetramers forming into dimers prior to volatilizing, and the mass loss rate being limited by the rate of dimer formation. Dimers would only form on the surface while the sample remains solid and the molecules in the bulk are locked in place. When the sample liquifies (above 210 °C), tetramers in the bulk gain sufficient freedom to dimerize, resulting in a faster rate of volatilization. The residual mass for **2** increased from 2% for 10 mg samples, to ~8% for 20 and 40 mg samples. Irregularities appeared in the derivative curves at ~200 °C aligning with decomposition observed when heating **2** under nitrogen atmosphere in capillaries (193–210 °C).

Comparing TGA experiments performed under similar conditions showed that **1**–**3** are more volatile than their corresponding mono- and bicyclic amidinates. The Ag triazenide **2** gave lower residual mass than the cyclic Ag amidinates (>10% for 10 mg samples).[5,22] As far as we know, the residual mass for **2** is the lowest reported for an exclusively Ag–N bonded

compound. Compound **1** performed on par with cyclic Cu amidinates in stress tests, however, while more volatile, the Cu triazenide **1** appeared less thermally stable than the cyclic amidinates.[21,40] The Au triazenide **3** gave a comparable residual mass to the cyclic Au amidinates (35% for **3**, compared to 40 and 25% for the mono- and bicyclic Au amidinate, respectively).[5,22] Interestingly, the Au triazenide **3** showed two nearly separated mass loss events, in contrast to the single step observed for the cyclic Au amidinates.

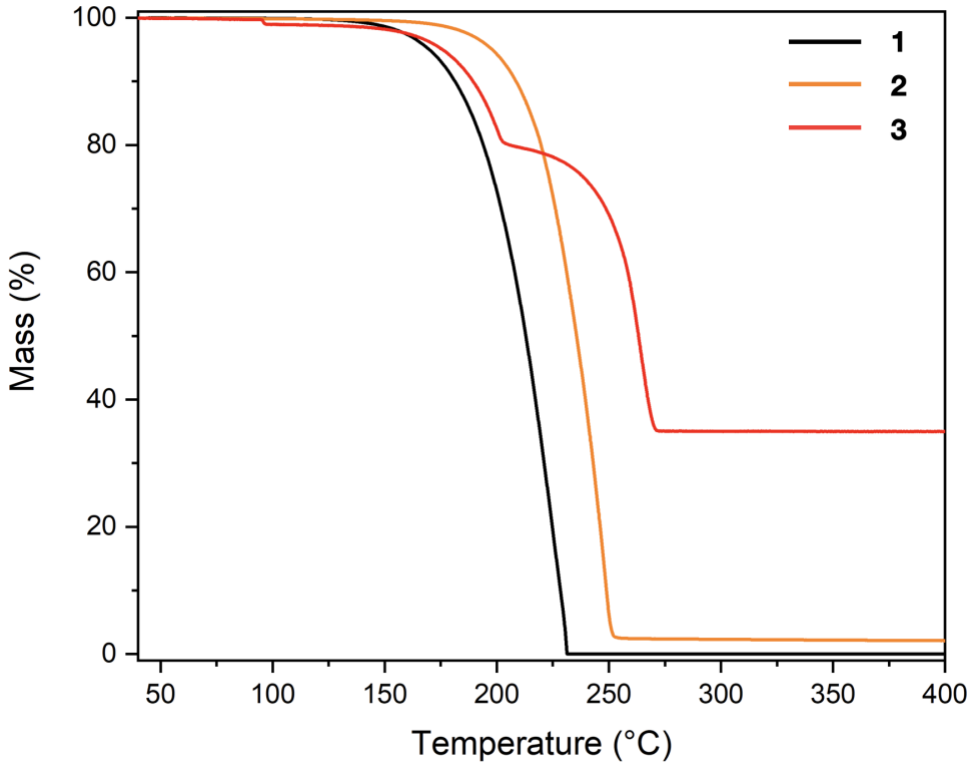

Figure 5: TGA ramp experiments for compounds **1**–**3** using 10 mg samples and a heating rate of 10 °C min^{-1}.

Differential scanning calorimetry (DSC) of **1**–**3** showed exotherms overlapping with their respective TGA mass loss events (Table 6). Compound **1** gave an exotherm between 190–215 °C. Compound **2** showed overlapping exotherms with multiple peaks between 196–250 °C. Compound **3** showed two exotherms, one between 200–220 °C, and a second between 230–290 °C. See the supporting information for the DSC plots.

Table 6: A summary of the thermal properties of compounds **1**–**3**. Temperatures are given in °C.

	Onset of Vola-tilization	Residual Mass (%)	Vac. Subl. Temp.	Decomp. Temp.	1st DSC Exo-therm	1 Torr VP Temp.
1	200	0	120–130	229–230	190–215	181 dimer 207
2	200	2	120–130	193–210	195–250	tetramer 213
3	175	35	120–130	150–155	190–220	–

Conclusions

In conclusion, we have presented the first example of volatile group 11 triazenides that are easy to prepare and purify. The crystal structure of **1** showed a dimer, whilst the **2** and **3** tetrameric with rhombic and buckled square conformations, respectively. NMR spectroscopy showed dimers for **1** and **3** while **2** gave a dimer/tetramer equilibrium. The compounds sublimed quantitively between 120 and 130 °C (at 0.5 mbar). By TGA, the Cu and Au triazenides **1** and **3** perform on par with their respective state of the art compounds in this class. Meanwhile, **2** volatilized at ~200 °C with 2% residual mass, which is an improvement over the cyclic Ag amidinates. DFT calculations showed a slight preference for dimeric **1** over tetrameric, in electronic energies. Conversely, **2** and **3** showed tetrameric preference. The Gibbs free energies from frequency calculations gave dimeric preference for **1**–**3**, increasing in the order **3** < **2** < **1**. Thus, **1**–**3** most likely form dimers when sublimed. NBO analysis showed that, from dimeric to rhombic, donor-acceptor interaction involving valence acceptors were destabilized (increasing in the order **3** < **2** < **1**), while those involving Rydberg acceptors were affected less. Tetramers where therefore favored by interactions that increase in number compared to two dimers (e.g. vicinal- and remote interactions), particularly interactions with Rydberg acceptor orbitals. However, in contrast to **2** and **3**, structures of **1** were unable to effectively use Rydberg acceptors and showed limited long-range interactions. In combination with being destabilized most, this may explain why crystals of **1** showed dimers while **2** and **3** showed tetramers. Overall, these compounds provide an easy-to-produce alternative to current state-of-the-art as potential CVD precursors. Furthermore, the ligands are easy to derivatize, allowing them to be tuned as desired.

Experimental Section

General Comments

Caution! As catenated nitrogen compounds are known to be associated with explosive hazards, tert-*butylazide, lithium (1,3-di-*tert-*butyltriazenide) and compounds **1–3** are possible explosive energetic materials. Although we have not experienced any difficulties or problems in the synthesis, characterization, sublimation and handling of these compounds, their energetic properties have not been investigated and are therefore unknown. We therefore highly recommend all appropriate standard safety precautions for handling explosive materials (safety glasses, face shield, blast shield, leather gloves, polymer apron and ear protection) be always used when working with these compounds.* All reactions and manipulations were carried out under a nitrogen atmosphere on a Schlenk line using Schlenk air-free techniques and in a Glovebox-Systemtechnik dry box. All anhydrous solvents were purchased from Sigma-Aldrich™ and further dried with 4Å molecular sieves. CuCl (99.995%), AgCl (99.999%), Me_2S•AuCl were purchased from Sigma-Aldrich™ and used without further purification. Lithium 1,3-di-*tert*-butyltriazenide was synthesized according to the literature procedure.[34] All NMR spectra were measured with an Oxford Varian and Bruker AvanceNeo 500 MHz spectrometers. Solvents peaks were used as an internal standard for the ^{1}H NMR and $^{13}C\{^{1}H\}$ NMR spectra. The decomposition points were determined in melting point tubes sealed under N_2 with a Stuart® SMP10 melting point apparatus and are uncorrected. Elemental analysis was performed by Mikroanalytisches Laboratorium Kolbe, Germany.

Synthesis of (1,3-di-*tert*-butyltriazenide)copper(I) 1

A solution of lithium 1,3-di-*tert*-butyltriazenide (4.95 g, 3.03 mmol) in THF (20 ml) was added to a suspension of CuCl (3.00 g, 3.03 mmol) in THF (80 mL) and the reaction was heated to 80 °C for 24 h in a pressure tube. After cooling down to room temperature, the mixture was concentrated under reduced pressure to give a yellow and brown solid residue. The residue was dissolved in *n*-hexane, filtered through a bed of Celite® and concentrated under reduced pressure to give the crude product as a solid. The crude was recrystallized from *n*-hexane at –35 °C to give **1** as a yellow solid (4.82 g, 72%).

1: Yellow crystals, mp: 229–230 °C. Sublimation: 120–130 °C (0.5 mbar). ^{1}H NMR (500 MHz, C_6D_6): δ 1.27 (s, 36H, C*H*$_3$, dimer). $^{13}C\{^{1}H\}$ NMR (125 MHz, C_6D_6): δ 30.8 (s, *C*H$_3$, dimer), 58.8 (s, *C*$_q$, dimer). Anal. calcd for $C_{16}H_{36}Cu_2N_6$: C, 43.72%; H, 8.25%; N, 19.12%. Found: C, 43.70%; H, 8.27%; N, 19.11%.

Synthesis of (1,3-di-*tert*-butyltriazenide)silver(I) 2

A solution of lithium 1,3-di-*tert*-butyltriazenide (8.56 g, 5.25 mmol) in THF (50 mL) was added to an aluminum foil wrapped reaction flask containing a solution of AgCl (7.52 g, 5.25 mmol) in THF (100 mL). The reaction mixture was stirred at room temperature for 48 h, then concentrated under reduced pressure to give a solid residue. The residue was purified by vacuum sublimation at 120–130 °C and 0.5 mbar to give **2** as a pale-yellow solid (10.4 g, 75%). For characterization, the sublimed solid of **2** (~1.0 g) was recrystallized from toluene at –35 °C.

2: Pale yellow crystals, decomp. 193–210 °C. Sublimation: 120–130 °C (0.5 mbar). ^{1}H NMR (500 MHz, C_6D_6, 13.3 mM): δ 1.27 (s, 36H, CH_3, dimer, 48%), 1.43 (s, 72H, CH_3, tetramer, 52%). ^{1}H NMR (500 MHz, THF-d_8, 13.3 mM): δ 1.21 (s, 36H, CH_3, dimer, 51%), 1.29 (s, 72H, CH_3, tetramer, 49%). ^{13}C{^{1}H} NMR (125 MHz, C_6D_6): δ 31.1 (CH$_3$, dimer), 32.0 (CH$_3$, tetramer), 58.3 (s, C_q, dimer), 60.5 (s, C_q, tetramer). Anal. calcd for $C_{32}H_{72}Ag_4N_{12}$: C, 36.38%; H, 6.87%; N, 15.91%. Found: C, 36.25%; H, 6.91%; N, 15.84%.

Synthesis of (1,3-di-*tert*-butyltriazenide)gold(I) 3

A solution of lithium 1,3-di-*tert*-butyltriazenide (0.28 g, 1.73 mmol) in THF (30 mL) was added to an aluminum-foil wrapped reaction flask containing a solution of (Me_2S)AuCl (0.51 g, 1.73 mmol) in THF (30 mL) at –78 ºC. The reaction mixture was stirred at –78 ºC for 30 min and at room temperature for 16 h, then concentrated under reduced pressure to give a solid residue. The residue was suspended in *n*-hexane, filtered through a pad of Celite® and concentrated under reduced pressure to give the crude product as a solid. The crude was recrystallized from *n*-hexane to give **3** as a solid (0.42 g, 70%).

3: Yellow crystals, decomp. 150–155 °C. Sublimation: 120–130 °C (0.5 mbar). ^{1}H NMR (500 MHz, C_6D_6): δ 1.27 (s, 36H, CH_3, dimer). ^{13}C{^{1}H} NMR (125 MHz, C_6D_6): δ 30.5 (s, CH$_3$, dimer), 62.5 (s, C_q, dimer). Anal. calcd for $C_{32}H_{72}Au_4N_{12}$: C, 27.20%; H, 5.14%; N, 11.90%. Found: C, 27.18%; H, 5.13%; N, 11.87%.

Variable Concentration and Temperature ^{1}H NMR Experiments with 2

For the variable concentration and temperature ^{1}H NMR experiments, solutions of nine different concentrations (1.9, 3.8, 5.7, 7.6, 9.5, 11.4, 13.3, 17.0 and 20.8 mM) were prepared by dissolving the required amount of **2** in 1.0 mL of C_6D_6. An ~400 µL aliquot of each solution was transferred to an NMR tube and used for ^{1}H NMR analysis. The samples were analyzed using 5 °C increments from +25 to +60 °C (see supporting information).

X-ray Crystallographic Analysis

Single crystals were obtained by recrystallization from *n*-hexane at –35 °C for **1** and **3**, and from toluene at –35 °C for **2**. The single crystals were used for X-ray diffraction data collection at 163 K for **1** and **2**, and 153 K for **3** on a Bruker D8 SMART Apex-II diffractometer, using graphite-monochromated Mo-Kα radiation (λ = 0.71073 Å). All data was collected in hemisphere with over 95% completeness to 2θ < 50.05°. The structures were solved by direct methods. The coordinates of metal atoms were determined from the initial solutions and the N and C atoms by subsequent differential Fourier syntheses. All non-hydrogen atoms were refined first in isotropic and then in anisotropic approximation using Bruker SHELXTL software. Selected crystal data are summarized below.

1: $C_{16}H_{36}Cu_2N_6$, M = 439.59, Orthorhombic, space group Pbca, a = 11.172(2), b = 10.683(2), c = 19.277(4) Å, V = 2300.7 $Å^3$, Z = 4, D_c = 1.269 cm^{-3}, μ = 1.858 mm^{-1}, T = 163 K, 2079 unique reflections measured, 1740 observed [$I > 2\sigma(I)$] , final $R1$ = 0.0355, wR2 (all data) = 0.1052, GOF = 0.921.

2: $C_{32}H_{72}Ag_4N_{12}$, M = 1056.48, Monoclinic, space group P2(1)/n, a = 11.726(6), b = 11.201(5), c = 17.369(8) Å, α = 90, β = 105.396(5), γ = 90°, V = 2199.5(2) $Å^3$, Z = 2, D_c = 1.595 cm^{-3}, μ = 1.790 mm^{-1}, T = 163 K, 3869 unique reflections measured, 3347 observed final [$I > 2\sigma(I)$], $R1$ = 0.0510, wR2 (all data) = 0.1465, GOF = 1.025.

3: $C_{32}H_{72}Au_4N_{12}$, M = 1412.88, Orthorhombic, space group P2(1)2(1)2(1), a = 10.445(4), b = 10.462(4), c = 41.456(14) Å, V = 4530(3) $Å^3$, Z = 4, D_c = 2.071 cm^{-3}, μ = 12.948 mm^{-1}, T = 153 K, 7925 unique reflections measured, 6320 observed [$I > 2\sigma(I)$], final $R1$ = 0.0921, wR2 (all data) = 0.2242, GOF = 0.996.

CCDC **2152400** for **1**, **2152401** for **2**, and **2152402** for **3** contain supplementary crystallographic data for this paper. These data can be obtained free of charge from the Cambridge Crystallographic Data Centre.

TGA

TGA was performed on Pt pans with a TA instrument Q50 analyzer housed in an MBraun Labmaster 130 dry box filled with N2 (99.998% purity). Pt pans were cleaned by

ultrasonication, first in dilute nitric acid (~3 M), then water and 2-propanol. The pans were heated in air by propane torch until red hot to remove any remaining impurities. All TGA experiments were performed under a flow of ultrapure N_2 (99.999%, 60 sccm). For ramp experiments, samples were heated to 500 °C at a rate of 10 °C min^{-1}. The Langmuir vapor pressure equations for **1** and **2** were derived from the TGA data with 10 mg of mass loading using a previously reported method[41] and employing benzoic acid as the calibrant.[42] The onset of volatilization was defined as the intersection between the tangent lines of the plateau and slope.

DSC Analysis

DSC experiments were performed using a TA Instruments DSC Q10 instrument. Inside a N_2 filled glovebox, samples of 0.30 ± 0.03 mg of **1**-**3** were sealed in Al pans. Unless otherwise stated, all samples were heated to 400 °C at a rate of 10 °C min^{-1} and N_2 (99.998%) was used as the purge gas. All experiments were performed in triplicate with similar mass loadings to ensure validity of the recorded data. Exothermic and endothermic events are indicated by positive and negative heat flow, respectively.

Quantum Chemical Computations

All quantum chemical calculations were preformed using Gaussian 16.[43] Geometry optimizations and harmonic normal mode vibrational calculations were performed using the long-range corrected hybrid DFT method LC-ωHPBE[44,45] and def2TZVP[46,47] basis set. Solvation was accounted for using the SMD continuum solvation model.[48] Minima were confirmed to have no imaginary frequencies. NBO analysis was performed on the minimized structures using NBO 7.1[49] interfaced from Gaussian 16.

Acknowledgements

This project was founded by the Swedish foundation for Strategic Research through the project "Time-resolved low temperature CVD for III-nitrides" (SSF-RMA 15-0018) and by the Knut and Alice Wallenberg foundation through the project "Bridging the THz gap" (No. KAW 2013.0049). L.O. acknowledges financial support from the Swedish Research Council (VR) and the Government Strategic Research Area in Materials Science on Functional Materials at Linköping University (Faculty Grant SFO Mat LiU no. 2009 00971).

References:

(1) Choi, T.-S.; Hess, D. W. Chemical Etching and Patterning of Copper, Silver, and Gold Films at Low Temperatures. *ECS J. Solid State Sci. Technol.* **2015**, *4*, N3084–N3093.

(2) Boysen, N.; Hasselmann, T.; Karle, S.; Rogalla, D.; Theirich, D.; Winter, M.; Riedl, T.; Devi, A. An N-Heterocyclic Carbene Based Silver Precursor for Plasma-Enhanced Spatial Atomic Layer Deposition of Silver Thin Films at Atmospheric Pressure. *Angew. Chem. Int. Ed.* **2018**, *57*, 16224.

(3) Mäkelä, M.; Hatanpää, T.; Mizohata, K.; Räisänen, J.; Ritala, M.; Leskelä, M. Thermal Atomic Layer Deposition of Continuous and Highly Conducting Gold Thin Films. *Chem. Mater.* **2017**, *29*, 6130–6136.

(4) Gordon, P. G.; Kurek, A.; Barry, S. T. Trends in Copper Precursor Development for CVD and ALD Applications. *ECS J. Solid State Sci. Technol.* **2015**, *4*, N3188–N3197.

(5) Coyle, J. P.; Gordon, P. G.; Wells, A. P.; Mandia, D. J.; Sirianni, E. R.; Yap, G. P. A.; Barry, S. T. Thermally Robust Gold and Silver Iminopyrrolidinates for Chemical Vapor Deposition of Metal Films. *Chem. Mater.* **2013**, *25*, 4566–4573.

(6) Lim, B. S.; Rahtu, A.; Gordon, R. G. Atomic Layer Deposition of Transition Metals. *Nat. Mater.* **2003**, *2*, 749–754.

(7) Lim, B. S.; Rahtu, A.; Park, J.-S.; Gordon, R. G. Synthesis and Characterization of Volatile, Thermally Stable, Reactive Transition Metal Amidinates. *Inorg. Chem.* **2003**, *42*, 7951–7958.

(8) Gordon, R. G. Atomic Layer Deposition for Semiconductors. In *Atomic Layer Deposition for Semiconductors*; Hwang, C. S., Yoo, C. Y., Eds.; Springer US: New York, 2014; pp 15–46.

(9) Coyle, J. P.; Kurek, A.; Pallister, P. J.; Sirianni, E. R.; Yap, G. P. A.; Barry, S. T.; Sun, Z. M. Preventing Thermolysis: Precursor Design for Volatile Copper Compounds. *Chem. Commun.* **2012**, *48*, 10440–10442.

(10) Barry, S. T. Amidinates, Guanidinates and Iminopyrrolidinates: Understanding Precursor Thermolysis to Design a Better Ligand. *Coord. Chem. Rev.* **2013**, *257*, 3192–3201.

(11) Li, Z.; Gordon, R. G.; Farmer, D. B.; Lin, Y.; Vlassak, J. Nucleation and Adhesion of ALD Copper on Cobalt Adhesion Layers and Tungsten Nitride Diffusion Barriers. *Electrochem. Solid-State Lett.* **2005**, *8*, G182–G185.

(12) Li, Z.; Rahtu, A.; Gordon, R. G. Atomic Layer Deposition of Ultrathin Copper Metal Films from a Liquid Copper(I) Amidinate Precursor. *J. Electrochem. Soc.* **2006**, *153*, C787.

(13) Dai, M.; Kwon, J.; Langereis, E.; Wielunski, L.; Chabal, Y. J.; Li, Z.; Gordon, R. G. In-Situ FTIR Study of Atomic Layer Deposition (ALD) of Copper Metal Films. *ECS Trans.* **2007**, *11*, 91–101.

(14) Kucheyev, S. O.; Biener, J.; Baumann, T. F.; Wang, Y. M.; Hamza, A. V.; Li, Z.; Lee, D. K.; Gordon, R. G. Mechanisms of Atomic Layer Deposition on Substrates with Ultrahigh Aspect Ratios. *Langmuir* **2008**, *24*, 943–948.

(15) Seitz, O.; Dai, M.; Aguirre-Tostado, F. S.; Wallace, R. M.; Chabal, Y. J. Copper−Metal Deposition on Self Assembled Monolayer for Making Top Contacts in Molecular Electronic Devices. *J. Am. Chem. Soc.* **2009**, *131*, 18159–18167.

(16) Ma, Q.; Guo, H.; Gordon, R. G.; Zaera, F. Uptake of Copper Acetamidinate ALD Precursors on Nickel Surfaces. *Chem. Mater.* **2010**, *22*, 352–359.

(17) Dai, M.; Kwon, J.; Halls, M. D.; Gordon, R. G.; Chabal, Y. J. Surface and Interface Processes during Atomic Layer Deposition of Copper on Silicon Oxide. *Langmuir* **2010**, *26*, 3911–3917.

(18) Guo, Z.; Li, H.; Chen, Q.; Sang, L.; Lizhen, Y.; Liu, Z.; Wang, X. Low-Temperature

Atomic Layer Deposition of High Purity, Smooth, Low Resistivity Copper Films by Using Amidinate Precursor and Hydrogen Plasma. *Chem. Mater.* **2015**, *27*, 5988–5996.
(19) Whitehorne, T. J. J.; Coyle, J. P.; Mahmood, A.; Monillas, W. H.; Yap, G. P. A.; Barry, S. T. Group 11 Amidinates and Guanidinates: Potential Precursors for Vapour Deposition. *Eur. J. Inorg. Chem.* **2011**, No. 21, 3240–3247.
(20) Chen, B.; Coyle, J. P.; Barry, S. T.; Zaera, F. Rational Design of Metalorganic Complexes for the Deposition of Solid Films: Growth of Metallic Copper with Amidinate Precursors. *Chem. Mater.* **2019**, *31*, 1681–1687.
(21) Beh, E. S.; Tong, L.; Gordon, R. G. Synthesis of 5,5-Bicyclic Amidines as Ligands for Thermally Stable Vapor Deposition Precursors. *Organometallics* **2017**, *36*, 1453–1456.
(22) Tong, L.; Davis, L. M.; Gong, X.; Feng, J.; Beh, E. S.; Gordon, R. G. Synthesis of Volatile, Reactive Coinage Metal 5,5-Bicyclic Amidinates with Enhanced Thermal Stability for Chemical Vapor Deposition. *Dalt. Trans.* **2019**, *48*, 6709–6713.
(23) Johnson, A. L.; Willcocks, A. M.; Richards, S. P. Synthesis and Structures of Group 11 Metal Triazenide Complexes: Ligand Supported Metallophilic Interactions. *Inorg. Chem.* **2009**, *48*, 8613–8622.
(24) Beck, J.; Strähle, J. Synthesis and Structure of 1,3-Diphenyltriazenidogold(I), a Tetrameric Molecule with Short Gold-Gold Distances. *Angew. Chem. Int. Ed. Engl.* **1986**, *25*, 95–96.
(25) Beck, J.; Strähle, J. Synthese Und Kristallstruktur von Bis [l , 5-DitolyIpentaazadienido-Silber (I)] Und Bis [l , 3-DiphenyItriazenido-SiIber (I)]. *Zeitschrift für Naturforsch.* **1986**, *41B*, 4–9.
(26) Hartmann, E.; Strähle, J. Synthese Und Struktur von 1,3-Bis(4-Trifluormethylphenyl)Triazenido-Komplexen Des Kupfer(I) Und Silber(I). *Zeitschrift für Naturforsch. B* **1988**, *43*, 818–824.
(27) Brown, I. D.; Dunitz, J. D. The Crystal Structure of Diazoaminobenzene Copper(I). *Acta Cryst.* **1961**, *14*, 480–485.
(28) Hartmann, E.; Strähle, J. 1,3-Bis(4-fluorphenyl)Triazenido-Komplexe von Kupfer Und Silber. Synthese Und Kristallstruktur von [Cu(F–C6H4N3C6H4–F)]4, [Ag(F–C6H4N3C6H4–F)]4 Und [Cu(F–C6H4N3C6H4–F)(OCH3)]4. *Z. anorg. allg. Chem.* **1990**, *583*, 31–40.
(29) O'Connor, J. E.; Janusonis, G. A.; Corey, E. R. The Molecular Structure of Tetrakis-[1,3-Dimethyltriazenocopper(I)]. *Chem. Commun. (London)* **1968**, No. 8, 445–446.
(30) Brinckman, F. E.; Haiss, H. S.; Robb, R. A. Metal-Nitrogen Bonding. Covalent Complexes of 1,3-Dimethyltriazene with Elements of Groups I, II, III, IV, and V. *Inorg. Chem.* **1965**, *4*, 936–942.
(31) O'Brien, N. J.; Rouf, P.; Samii, R.; Rönnby, K.; Buttera, S. C.; Hsu, C.-W.; Ivanov, I. G.; Kessler, V.; Ojamäe, L.; Pedersen, H. In-Situ Activation of an Indium(III) Triazenide Precursor for Epitaxial Indium Nitride by Atomic Layer Deposition. *Chem. Mater.* **2020**, *32*, 4481–4489.
(32) Rouf, P.; Samii, R.; Rönnby, K.; Bakhit, B.; Buttera, S. C.; Martinovic, I.; Ojamäe, L.; Hsu, C.-W.; Kessler, V.; Palisaitis, J.; Kessler, V.; Pedersen, H.; O'Brien, N. J. Hexacoordinated Gallium(III) Triazenide Precursor for Epitaxial Gallium Nitride by Atomic Layer Deposition. *Chem. Mater.* **2021**, *33*, 3266–3275.
(33) Samii, R.; Zanders, D.; Buttera, S. C.; Kessler, V.; Ojamäe, L.; Pedersen, H.; O'Brien, N. J. Synthesis and Thermal Study of Hexacoordinated Aluminum(III) Triazenides for Use in Atomic Layer Deposition. *Inorg. Chem.* **2021**, *60*, 4578–4587.
(34) Samii, R.; Zanders, D.; Fransson, A.; Bačić, G.; Barry, S. T.; Ojamäe, L.; Kessler, V.;

Pedersen, H.; O'Brien, N. J. Synthesis, Characterization and Thermal Study of Divalent Germanium, Tin and Lead Triazenides as Potential Vapor Deposition Precursors. *Inorg. Chem.* **2021**, *60*, 12759–12765.
(35) Rouf, P.; Palisaitis, J.; Bakhit, B.; O'Brien, N. J.; Pedersen, H. In0.5Ga0.5N Layers by Atomic Layer Deposition. *J. Mater. Chem. C* **2021**, *9*, 13077–13080.
(36) Mpofu, P.; Rouf, P.; O'Brien, N. J.; Forsberg, U.; Pedersen, H. Thermal Atomic Layer Deposition of In2O3 Thin Films Using a Homoleptic Indium Triazenide Precursor and Water. *ChemRxiv* **2021**.
(37) Vliet, P. I. V.; Koten, G. Van; Vrieze, K. Complexes of N,N′-Substituted Formamidines I. Compounds [M(RNC(H)NR′)]n (M = CuI, AgI; R = p-TOLYL; R′ = ALKYL; n = 2,4); and Study of the Dimer–Dimer and Dimer–Tetramer Equilibria in Solution. *J. Organomet. Chem.* **1979**, *179*, 89–100.
(38) Abdou, H. E.; Mohamed, A. A.; Fackler, J. P. Synthesis, Characterization, Luminescence, and Electrochemistry of New Tetranuclear Gold(I) Amidinate Clusters: Au4[PhNC(Ph)NPh]4, Au4[PhNC(CH3)NPh]4, and Au 4[ArNC(H)NAr]4. *J. Clust. Sci.* **2007**, *18*, 630–641.
(39) Irwin, M. D.; Abdou, H. E.; Mohamed, A. A.; Fackler, J. P. Synthesis and X-Ray Structures of Silver and Gold Guanidinate-like Complexes. A Au(II) Complex with a 2.47 Å Au-Au Distance. *Chem. Commun.* **2003**, 2882–2883.
(40) Coyle, J. P.; Pallister, P. J.; Kurek, A.; Sirianni, E. R.; Yap, G. P. A.; Barry, S. T. Copper Iminopyrrolidinates: A Study of Thermal and Surface Chemistry. *Inorg. Chem.* **2013**, *52*, 910–917.
(41) Kunte, G. V.; Shivashankar, S. A.; Umarji, A. M. Thermogravimetric Evaluation of the Suitability of Precursors for MOCVD. *Meas. Sci. Technol.* **2008**, *19*, 025704.
(42) Wright, S. F.; Phang, P.; Dollimore, D.; Alexander, K. S. An Overview of Calibration Materials Used in Thermal Analysis—Benzoic Acid. *Thermochim. Acta* **2002**, *392–393*, 251–257.
(43) Frisch, M. J.; Trucks, G. W.; Schlegel, H. B.; Scuseria, G. E.; Robb, M. A.; Cheeseman, J. R.; Scalmani, G.; Barone, V.; Petersson, G. A.; Nakatsuji, H.; Li, X.; Caricato, M.; Marenich, A. V.; Bloino, J.; Janesko, B. G.; Gomperts, R.; Mennucci, B.; Hratchian, H. P.; Ortiz, J. V.; Izmaylov, A. F.; Sonnenberg, J. L.; Williams-Young, D.; Ding, F.; Lipparini, F.; Egidi, F.; Goings, J.; Peng, B.; Petrone, A.; Henderson, T.; Ranasinghe, D.; Zakrzewski, V. G.; Gao, J.; Rega, N.; Zheng, G.; Liang, W.; Hada, M.; Ehara, M.; Toyota, K.; Fukuda, R.; Hasegawa, J.; Ishida, M.; Nakajima, T.; Honda, Y.; Kitao, O.; Nakai, H.; Vreven, T.; Throssell, K.; Montgomery, J. A., J.; Peralta, J. E.; Ogliaro, F.; Bearpark, M. J.; Heyd, J. J.; Brothers, E. N.; Kudin, K. N.; Staroverov, V. N.; Keith, T. A.; Kobayashi, R.; Normand, J.; Raghavachari, K.; Rendell, A. P.; Burant, J. C.; Iyengar, S. S.; Tomasi, J.; Cossi, M.; Millam, J. M.; Klene, M.; Adamo, C.; Cammi, R.; Ochterski, J. W.; Martin, R. L.; Morokuma, K.; Farkas, O.; Foresman, J. B.; Fox, D. J. Gaussian 16 Revision B.01. 2016.
(44) Hanson-Heine, M. W. D.; George, M. W.; Besley, N. A. Calculating Excited State Properties Using Kohn-Sham Density Functional Theory. *J. Chem. Phys.* **2013**, *138*, 064101.
(45) Henderson, T. M.; Izmaylov, A. F.; Scalmani, G.; Scuseria, G. E. Can Short-Range Hybrids Describe Long-Range-Dependent Properties? *J. Chem. Phys.* **2009**, *131*, 044108.
(46) Weigend, F.; Ahlrichs, R. Balanced Basis Sets of Split Valence, Triple Zeta Valence and Quadruple Zeta Valence Quality for H to Rn: Design and Assessment of Accuracy. *Phys. Chem. Chem. Phys.* **2005**, *7*, 3297–3305.
(47) Metz, B.; Stoll, H.; Dolg, M. Small-Core Multiconfiguration-Dirac-Hartree-Fock-

Adjusted Pseudopotentials for Post-d Main Group Elements: Application to PbH and PbO. *J. Chem. Phys.* **2000**, *113*, 2563–2569.
(48) Marenich, A. V.; Cramer, C. J.; Truhlar, D. G. Universal Solvation Model Based on Solute Electron Density and on a Continuum Model of the Solvent Defined by the Bulk Dielectric Constant and Atomic Surface Tensions. *J. Phys. Chem. B* **2009**, *113*, 6378–6396.
(49) Glendening, E. D.; Badenhoop, J. K.; Reed, A. E.; Carpenter, J. E.; Bohmann, J. A.; Morales, C. M.; Karafiloglou, P.; Landis, C. R.; Weinhold, F. NBO 7.0. *NBO 7.0* University of Wisconsin, Madison, WI (2018).